

Modeling of Plasmon Resonances of Multiple Flat Noble-Metal Nanostrips With a Median-Line Integral Equation Technique

Olga V. Shapoval, *Student Member, IEEE*, Ronan Sauleau, *Senior Member, IEEE*,
and Alexander I. Nosich, *Fellow, IEEE*

Abstract—The surface plasmon and the periodicity-induced resonances in the scattering and absorption of light by multiple flat nanosize noble-metal strips are investigated using a new efficient model. It exploits the fact that the nanostrip thickness is a small fraction of the wavelength in the visible range. This justifies shrinking the strip cross section to its median line and using the generalized boundary conditions on that line, with the strip thickness entering the coefficients. As a result, the scattering problem is reduced to the singular and hypersingular integral equations. We discretize them using quadrature formulas of interpolation type and build an algorithm having guaranteed convergence and controlled accuracy of computations. It enables fast simulation of structures consisting of many noble-metal strips. Near- and far-field characteristics for finite flat grating of silver and gold nanostrips are presented.

Index Terms—Absorption, noble-metal strips, Nystrom method, optical antennas, scattering, singular and hypersingular integral equations (IEs), surface plasmon resonance.

I. INTRODUCTION

Noble-metal nanosize strips illuminated by a transversely polarized light are known to display intensive localized surface-plasmon resonances (PRs) in the visible and far-infrared ranges [1]–[8]. They are attractive as easily manufactured components of optical antennas and sensors. The typical dimensions of metal nanostrips are the width from 100 to 1000 nm and the thickness from 5 to 40 nm. Thereby, the thickness is some 8 to 180 times smaller than the wavelength in the whole visible band (300 to 900 nm). PRs can be easily revealed by measuring or computing the scattering and absorption of light by noble-metal strips.

The computational methods used for the optical modeling of nanostrips include volume [1], [4] and boundary [3]–[6]

integral equations (IEs), where the integration domain is the area of the strip cross section and its closed contour, respectively. Here, boundary IEs are considered more efficient as they imply the discretization of the boundary instead of the area; still typical number of unknowns is hundreds and thousands, respectively [3]–[6]. More essentially, boundary IEs can be cast, unlike volume IEs, to the forms having nonsingular and integrable kernels and thus can be discretized more reliably. Still many forms of the boundary IEs possess spurious eigenvalues [9]; this spoils the performance of the boundary IEs of [3]–[6] for the strips wider than half-wavelength of the incident light that corresponds to the first spurious eigenvalue for a strip of subwavelength thickness. To avoid this, one should use the so-called Muller's boundary IE; still the shape of the contour and its nonsmoothness greatly affects the rate of convergence of corresponding algorithms. All mentioned becomes even more important for multiple metal strips.

Our suggestion is that, in the case of the strip thickness being only a small fraction of the free-space wavelength, the analysis can be simplified by neglecting the internal field and considering only the external field limit values. This enables reduction of the integration contour to the strip median line and thus leads to more economic numerical technique. This idea is not new as it has been exploited in [10]–[18] in relation to the shells and strips of conventional dielectrics; however, it has not been yet applied to the noble-metal nanostrips in the visible range. We have recently developed a novel Nystrom-type discretization of the median-line IEs and applied it to the scattering by dielectric strips [19]. In the conference papers [20], [21], we have presented preliminary results for the standalone and several strips of noble metals; thus, the aim of this paper is a more detailed and conclusive presentation of this topic. In nanooptics, our approach opens possibility of reliable modeling of the scatterers consisting of dozens and hundreds of noble-metal strips such as multifrequency optical antenna arrays, plasmonic sensors, and plasmonic solar cells.

The remainder of this paper is organized as follows. Section II briefly reviews the generalized boundary conditions (GBC), the main points of the median-line IE method, and the Nystrom-type discretization; to save space, we make extensive references to [19]. Section III contains main formulas of the scattering characteristics. In Section IV, we present numerical results related mainly to the PR-assisted scattering by flat arrays of silver and gold strips and discuss the field behavior in the near and far zones. The appearance of the grating resonances on long grating of strips is also demonstrated. Conclusions are summarized

Manuscript received March 16, 2012; revised November 30, 2012; accepted March 25, 2013. Date of publication April 3, 2013; date of current version May 6, 2013. This work was supported in part by the National Academy of Sciences of Ukraine via the State Target Program "Nanotechnologies and Nanomaterials" and the European Science Foundation via the Research Networking Programme "Newfocus." The review of this paper was arranged by Associate Editor Y.-H. Cho.

O. V. Shapoval and A. I. Nosich are with the Institute of Radio-Physics and Electronics, National Academy of Sciences of Ukraine, Kharkiv 61085, Ukraine (e-mail: olga.v.shapoval@gmail.com; anosich@yahoo.com).

R. Sauleau is with the Institute of Electronics and Telecommunications of Rennes, Universite de Rennes 1, Rennes Cedex 35042, France (e-mail: ronan.sauleau@univ-rennes1.fr).

Color versions of one or more of the figures in this paper are available online at <http://ieeexplore.ieee.org>.

Digital Object Identifier 10.1109/TNANO.2013.2256365

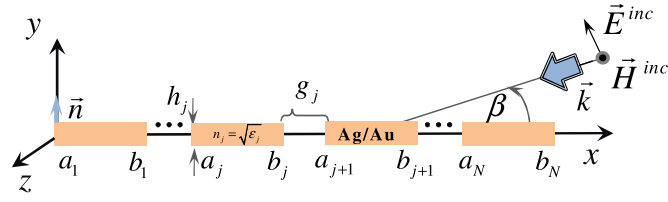


Fig. 1. Geometry of finite, not necessarily periodic planar multistrip grating.

in Section V. In the paper, the time dependence $\sim e^{-i\omega t}$ is assumed.

II. GBCS AND MEDIAN-LINE INTEGRAL EQUATIONS

A. Formulation and GBCs

Consider the H-polarized electromagnetic plane wave incident at the angle β on a flat coplanar ensemble of N silver nanostrips of the dielectric permittivity ε_j , width d_j , thickness h_j , and separated with gaps g_j . The corresponding freestanding geometry and the problem notations are shown in Fig. 1. The strips are assumed infinite along the z -axis. Note that this configuration is not a limitation for the method used, and each strip can be located arbitrarily in the xy plane. In the case of the identical multistrip configuration, we assume that $\varepsilon_j = \varepsilon$, $d_j = d$, $h_j = h$, and $g_j = g$ for all $j = 1, \dots, N$.

The incident wave field is given as $H_z^{\text{inc}}(\vec{r}) = e^{-ik(x \cos \beta + y \sin \beta)}$ where $\vec{r} = (x, y)$, $k = \omega/c = 2\pi/\lambda$, and λ is the free-space wavelength. In the presence of strips, the total field is a sum of this function and the scattered field $H_z^{\text{sc}}(\vec{r})$. The latter must satisfy the corresponding Helmholtz equation inside and outside the strips and the tangential components' continuity across strips' contours of cross section. Besides, $H_z^{\text{sc}}(\vec{r})$ must satisfy Sommerfeld radiation condition and if the strip contour has edges, the condition of the local energy finiteness. Such a scattering problem is uniquely solvable.

Now, keeping in mind that $h_j \ll \lambda$ in the visible range, we neglect the internal fields inside the strips and impose the two-side GBCs for the external field limiting values at the strip median lines $S = \bigcup_{j=1}^N S_j$, where $S_j = \{(x, 0) : x \in [a_j, b_j]\}$, and a_j and b_j are the strip endpoints

$$\begin{aligned} \partial[H_z^+(\vec{r}) + H_z^-(\vec{r})]/\partial\vec{n} &= -i2kR[H_z^+(\vec{r}) - H_z^-(\vec{r})] \\ [H_z^+(\vec{r}) + H_z^-(\vec{r})] &= i2Qk^{-1}\partial[H_z^+(\vec{r}) - H_z^-(\vec{r})]/\partial\vec{n}. \end{aligned} \quad (1)$$

Here, \vec{n} is the unit vector normal to the strip top side, the indices \pm correspond to the limit values of the field at the top and bottom sides of the strip, respectively, and R_j and Q_j ($j = 1, \dots, N$) are the electric and magnetic resistivities

$$R_j = i(\nu_j^{-1}/2) \cot(kh_j\nu_j/2), \quad Q_j = i(\nu_j/2) \cot(kh_j\nu_j/2) \quad (2)$$

which depend on the refractive index $\nu_j = \varepsilon_j^{1/2}$, thickness, and frequency. The formulas (1) and (2) have been derived for $kh_j \ll 1$ and $|\varepsilon_j| \gg 1$ in several papers, first in [9] and, independently, in [11]–[13]. They had been cast to the form (1) in [14]. Modification of (2) needed to adapt the resistivities to the small contrast case $|\varepsilon_j - 1| \ll 1$ was proposed in [15].

To keep the uniqueness of solution after the reduction of strips to their median lines, we have to add the condition of finiteness of power contained in finite domain. This limits allowed field singularities at the strip endpoints. Note that earlier GBC (1) were used in the analysis of wave scattering by infinite flat gratings of dielectric and impedance strips [16]–[18] and by standalone strips of conventional dielectrics [19]. Their validation was performed in [15] using the volume IE.

B. Singular Integral Equations

To satisfy Helmholtz equation and radiation condition, we seek the scattered field as a sum of single-layer and double-layer potentials

$$\begin{aligned} H_z^{\text{sc}}(\vec{r}) &= \sum_{j=1}^N \left[k \int_{S_j} v_j(\vec{r}') G(\vec{r}, \vec{r}') d\vec{r}' \right. \\ &\quad \left. + \int_{S_j} w_j(\vec{r}') \frac{\partial G(\vec{r}, \vec{r}')}{\partial \vec{r}'} d\vec{r}' \right] \end{aligned} \quad (3)$$

where $G(\vec{r}, \vec{r}') = (i/4)H_0^{(1)}(k|\vec{r} - \vec{r}'|)$ is the Green function. Note that the unknown functions $v_j(\vec{r})$ are $w_j(\vec{r})$ are magnetic and electric currents, respectively, induced on the strips.

Using GBC (1) and the properties of the limit values of potentials in (3), we obtain two independent sets of IEs of the second kind. One of them contains equations with logarithmic-type singularities for $v_l(x)$, and another with hypertype singularities for $w_l(x)$, $l = 1, \dots, N$

$$\begin{aligned} 4Q_l v_l(x_0^l) + k \sum_{j=1}^N \int_{a_j}^{b_j} v_j(x) H_0^{(1)}(k|x - x_0^l|) dx \\ = 4ie^{-ikx_0^l \cos \beta} \\ 4R_l w_l(x_0^l) + \sum_{j=1}^N \int_{a_j}^{b_j} w_j(x) \frac{H_1^{(1)}(k|x - x_0^l|)}{|x - x_0^l|} dx \\ = 4 \sin \beta e^{-ikx_0^l \cos \beta}. \end{aligned} \quad (4)$$

These IEs are generalization of (5) and (6) of [19] to the case of flat multiple-strip configuration, and the integral terms in (5) are understood in the sense of finite part of Hadamard.

C. Nystrom-Type Discretization

Changing the variables as $x^j = d_j t/2 + (b_j + a_j)/2$ and similarly for x_0^l , and introducing $\rho_{jl}(t, t_0) = k|x^j(t) - x_0^l(t_0)|$ and new unknown functions as $\tilde{w}_j(t) = w_j(t)(1 - t^2)^{-1/2}$, we get

$$\begin{aligned} 4Q_l v_l(t_0) + \kappa_l \int_{-1}^1 v_l(t) H_0^{(1)}(\kappa_l |t - t_0|) dt \\ + \sum_{j=1, j \neq l}^N \kappa_j \int_{-1}^1 v_j(t) K_j^v(\rho_{jl}(t, t_0)) dt = f_v^l(t_0), \quad l = 1, \dots, N \end{aligned} \quad (6)$$

$$\begin{aligned}
& 4R_l \tilde{w}_l(t_0) \sqrt{1-t_0^2} + \int_{-1}^1 \tilde{w}_l(t) \sqrt{1-t^2} \frac{H_1^{(1)}(\kappa_l |t-t_0|)}{|t-t_0|} dt \\
& + \sum_{j=1, \neq l}^N d_j \int_{-1}^1 \tilde{w}_j(t) \sqrt{1-t^2} K_j^w(\rho_{jl}(t, t_0)) dt \\
& = f_w^l(t_0), \quad l = 1, \dots, N
\end{aligned} \quad (7)$$

where $K_j^v(\rho_{jl}(t, t_0))$, $f_v^l(t_0)$ and $K_j^w(\rho_{jl}(t, t_0))$, $f_w^l(t_0)$ for $j, l = 1, \dots, N$ are regular functions, and $\kappa_j = \pi d_j / \lambda$.

Following [19], we isolate the singularities and discretize the resulted sets of IEs using Nystrom-type method with two different quadrature rules of interpolation type. For IEs (6), we use the Gauss–Legendre quadrature formulas of the n_v th order with nodes in the nulls of Legendre polynomials $P_{n_v}(\tau_j) = 0$, $j = 1, \dots, n_v$ for the singular and regular parts

$$\int_{-1}^1 v_j(t) \ln |t-t_0| dt = \sum_{i=1}^{n_v} A_i^{n_v} S(\tau_i, t_0) v_j(\tau_i) \quad (8)$$

$$\int_{-1}^1 v_j(t) R_v(t, t_0) dt = \sum_{i=1}^{n_v} A_i^{n_v} v_j(\tau_i) R(\tau_i, t_0) \quad (9)$$

where

$$\begin{aligned}
S(t, t_0) &= \frac{1}{2} \ln(1-t_0^2) + L_1(t_0) \\
&+ \sum_{l=1}^{n_v-1} P_l(t) [L_{l+1}(t_0) - L_{l-1}(t_0)] \quad (10)
\end{aligned}$$

$$A_i^{n_v} = 2/[P'_{n_v}(\tau_i)^2(1-\tau_i^2)] \quad (11)$$

and $L_l(t)$ is the Legendre function of the first order.

For IEs (7), Gauss–Chebyshev quadrature formulas of the n_w th order (with the weight $(1-t^2)^{1/2}$) are more efficient, with nodes in the nulls of Chebyshev polynomials of the second kind, $t_j = \cos(\pi j/n_w)$, $j = 1, \dots, n_w$. These formulas have the following form for the hypersingular, log-singular, and regular integrals met in (7)

$$\begin{aligned}
& \int_{-1}^{+1} \frac{\tilde{w}_j(t)}{(t-t_0)^2} \sqrt{1-t^2} dt = \frac{\pi}{n_w+1} \sum_{i=1, i \neq j}^{n_w} \tilde{w}_j(t_i) \\
& \times \frac{(1-t_i^2)(1-(-1)^{i+s})}{(t_i-t_0)^2} - \frac{\pi(n_w+1)}{2} \tilde{w}_j(t_0) \quad (12)
\end{aligned}$$

$$\begin{aligned}
& \int_{-1}^{+1} \tilde{w}_j(t) \ln |t-t_0| \sqrt{1-t^2} dt = \frac{\pi}{(n_w+1)} \sum_{i=1}^{n_w} \tilde{w}_j(t_i) (t_i^2 - 1) \\
& \times \left[\ln 2 + 2 \sum_{k=1}^{n_w} \frac{T_k(t_i) T_k(t_0)}{k} + \frac{(-1)^i}{n_w+1} T_{n_w}(t_0) \right] \quad (13)
\end{aligned}$$

$$\begin{aligned}
& \int_{-1}^{+1} \tilde{w}_j(t) R_w(t, t_0) \sqrt{1-t^2} dt \\
& = \frac{\pi}{n_w+1} \sum_{i=1}^{n_w} \tilde{w}_j(t_i) R_w(t_i, t_0) (1-t_i^2). \quad (14)
\end{aligned}$$

Here, $R_v(t, t_0)$, $R_w(t, t_0)$ can be arbitrary regular functions on the interval $[-1, 1]$, and $T_l(t)$ is the Chebyshev polynomial

of the second kind. As the collocation nodes, we choose the corresponding discretization nodes.

Applying the above presented quadrature formulas, we arrive at two independent sets of matrix equations of the orders n_v and n_w , respectively, for the values $v_j(\tau_i)$ and $\tilde{w}_j(t_k)$. These matrix equations represent discrete model of our SIEs (4) and (5). On solving them numerically, we obtain approximate solutions to our IEs in the form of interpolation polynomials for the unknown surface currents.

The chosen quadrature formulas ensure rapid convergence of numerical solutions to the accurate ones if $n_v, n_w \rightarrow \infty$. Conservative estimation gives the rates of convergence as $O(1/n_{v,w})$, although the actual rate is always greater [19]. For instance, to achieve four-digit accuracy in the analysis of a 2λ -wide silver strip, one can take $n_v = n_w = 20$. Such techniques are known as Nystrom methods [22] and also as the methods of discrete singularities [23].

III. SCATTERING CHARACTERISTICS

Using the large-argument asymptotics for the Hankel functions in the kernels of (4), the scattered magnetic field in the far zone can be represented as $H_z^{sc} \sim (2/i\pi kr)^{1/2} e^{ikr} \Phi(\varphi)$, where $\Phi(\varphi)$ is the radiation pattern. It is found as

$$\Phi(\varphi) = (ik/4) \sum_{j=1}^N \int_{S_j} [v_j(x) - i \sin \varphi w_j(x)] e^{-ikx \cos \varphi} dx. \quad (15)$$

The total scattering cross section (TSCS) and the absorption cross section (ACS) are determined as follows:

$$\sigma_{sc} = (2/\pi k) \int_0^{2\pi} |\Phi(\varphi)|^2 d\varphi \quad (16)$$

$$\sigma_{abs} = \sum_{j=1}^N \int_{S_j} [\text{Re } Q_j |v_j(x)|^2 + \text{Re } R_j |w_j(x)|^2] dx. \quad (17)$$

Their sum is the extinction cross section, and the optical theorem tells that $\sigma_{sc} + \sigma_{abs} = -(4/k) \text{Re} \Phi(\beta + \pi)$.

IV. NUMERICAL RESULTS AND DISCUSSION

Using the above presented technique, we have analyzed the scattering and absorption characteristics of standalone and multiple nanosize silver and gold strips and investigated the influence of the angle of incidence, strip thickness, and strip and gap width on the resonances (see Figs. 2–10). To characterize the complex dielectric permittivity of silver and gold, we took the experimental data of [24] and used an Akima cubic spline interpolation to eliminate the wiggles in the interpolant.

A. Stand-Alone Strip

The plots of the normalized TSCS and ACS of a standalone (solid curves) thin flat silver strip, computed after solving (4) and (5) with uniform accuracy of 10^{-4} , are shown in Fig. 2(a) and (b), respectively, as a function of the wavelength at inclined incidence of a plane wave. Note that the smaller λ resonance peaks are better visible on the ACS curves than TSCS ones. This can be used for their more reliable detection.

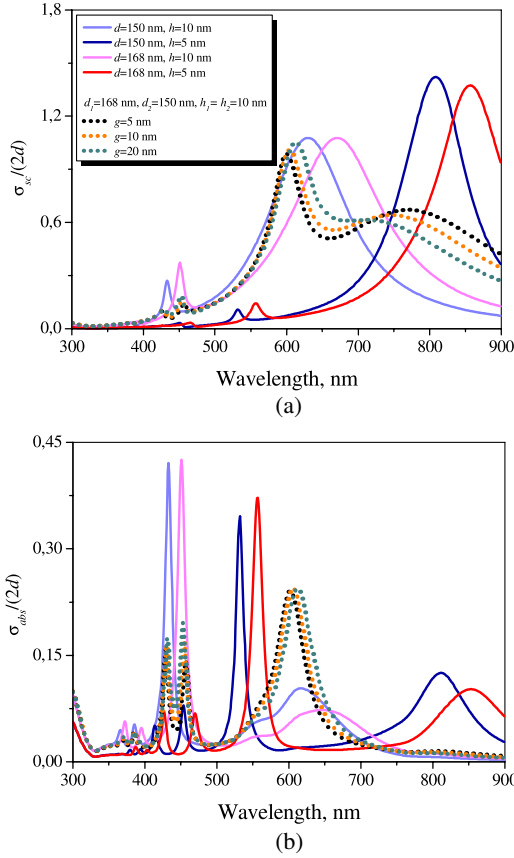


Fig. 2. (a) Normalized TSCS and (b) ACS as a function of the wavelength for standalone silver strips (solid curves) and combination of $N = 2$ strips (dotted curves) of different widths, thicknesses, and gaps at the inclined ($\beta = \pi/4$) incidence; $n_w = n_v = 20$.

An important question is what an error is in replacing a rectangular cross section of the strip with its median line. Comparison of the TSCS curve for the strip with $d = 168$ nm, $h = 10$ nm at $\beta = \pi/4$ in Fig. 2(a) with the corresponding curve in [5] calculated using a boundary IE on a rectangular contour with the same h and d and rounded corners shows a close agreement. The discrepancy between two curves is less than 5% in the studied range. In fact, our results may be more accurate than those of [3]–[7] as our algorithm’s convergence has been proven theoretically (see for details [19]) while the specific forms of the IE used in [3]–[7] do not amend themselves for such a mathematical proof. Here, we understand the convergence in mathematical sense, as possibility of reducing the error of computations by solving progressively larger matrices (many divergent schemes still yield a few correct digits in solution).

Fig. 3(a)–(d) displays the total near-field and, in the insets, the scattered far-field patterns in the first- to the fourth-order PRs H_n ($n = 1, 2, 3, 4$), respectively, for the strip of $d = 150$ nm and $h = 5$ nm. These are the Fabry–Perot-like resonances on the short-range surface plasmon wave of a silver slab traveling between the strip edges [5]–[8]. Note that the even-index resonances can be excited only at the inclined incidence because of their modal field antisymmetry across the y -axis.

The curves in Fig. 4 emphasize the properties of the PRs in dependence of the strip width and material. Here, the H_1

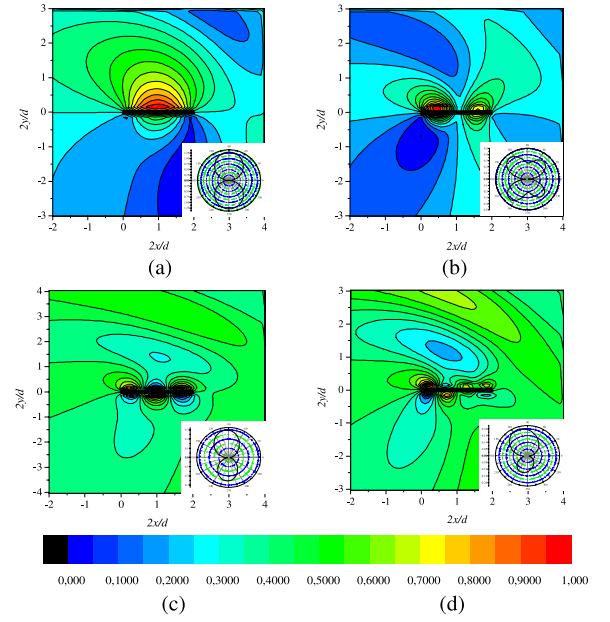


Fig. 3. Scattered magnetic far-field (insets) and total magnetic near-field patterns ($\beta = \pi/4$) for standalone silver strips with $d = 150$ nm, $h = 5$ nm in the plasmon resonances at (a) $\lambda = 813$ nm, (b) 533 nm, (c) 453 nm, (d) and 415 nm.

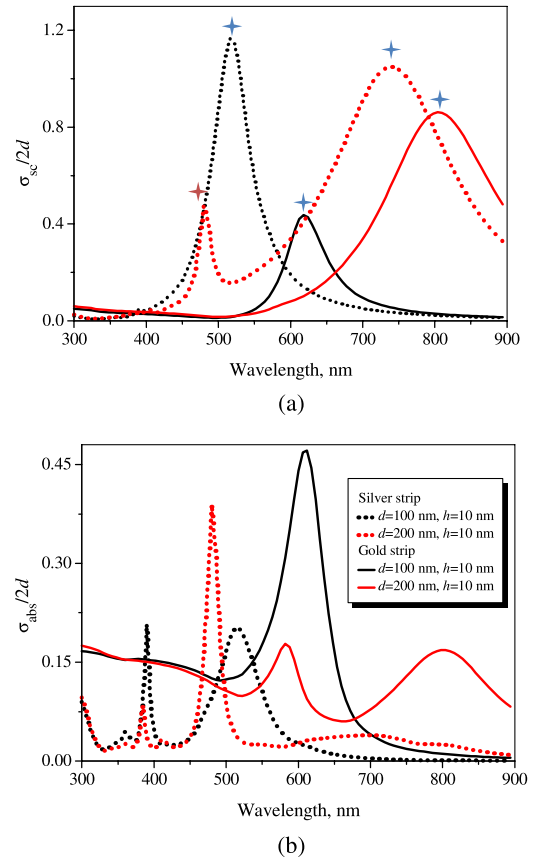


Fig. 4. (a) Normalized TSCS and (b) ACS as a function of the wavelength for standalone silver (dotted curves) and gold (solid curves) strips of thickness $h = 10$ nm versus the strips width; other parameters are $\beta = \pi/4$, $n_v = n_w = 20$.

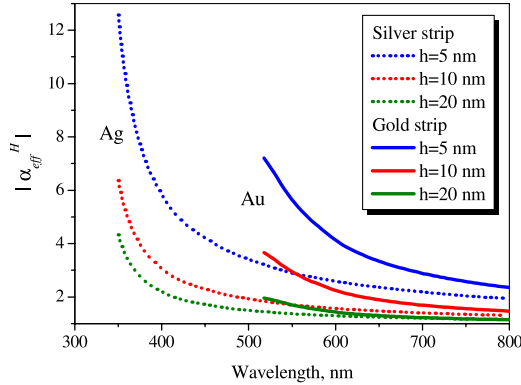


Fig. 5. Absolute value of the normalized effective refractive index $|\alpha_{\text{eff}}^H|$ versus the wavelength, for the short-range surface plasmon wave propagating along the silver (dotted curves) and gold (solid curves) slabs of different thicknesses located in free space.

resonances are denoted by blue diamonds and the H_2 ones by red ones. One can see that shorter strips like a 100-nm-wide silver (black dotted curve) or gold strip (black solid curve) commonly support only the first-order PR in the visible band.

Wider strips can support two PRs in the same range. Again, higher order resonances are more pronounced on the ACS dependences than on the TSCS ones.

B. Effective Refractive Index of the Strip and PR Prediction

To obtain a better insight into the nature of PRs on the individual nanostrips in free space, it is instructive to calculate so-called effective refractive index of the short-range surface plasmon modes [5], [6]. This value is defined as the normalized propagation constant (wavenumber) of the thin silver-slab mode having x -odd magnetic field. Within our model, it can be found explicitly as

$$\alpha_{\text{eff}}^H = (1 - 4R^2)^{1/2} \quad (18)$$

after the use of GBC (1). Note that it depends on the wavelength and strip thickness.

In Fig. 5, we present calculated effective refractive indices of short-range surface plasmon waves propagating along the silver (dotted curves) and gold (solid curves) strips of different thickness from 5 to 20 nm.

Then, the resonance values of the strip width are found to satisfy the equation typical for a Fabry–Perot resonance

$$kd\alpha_{\text{eff}}(\lambda, h, \varepsilon) = m\pi - \varphi \quad (19)$$

where φ is associated with the phase of the wave reflection from the strip edge [6]. In Fig. 6, we present the comparison of the resonances predicted by this simple equation (with φ found from fitting at a central wavelength) and obtained by computations, for the silver strips of the same thickness as in Fig. 5.

Two main aspects have an effect on the agreement between phase estimation from data computed via proposed Nystrom-type discretization and mentioned above linear fitting. As can be seen from Fig. 6, the thinner strips and their associated higher order PR provide a better agreement. Thus, correctly matched phase long estimation and short-range surface plasmon resonance condition (19) give an opportunity to predict

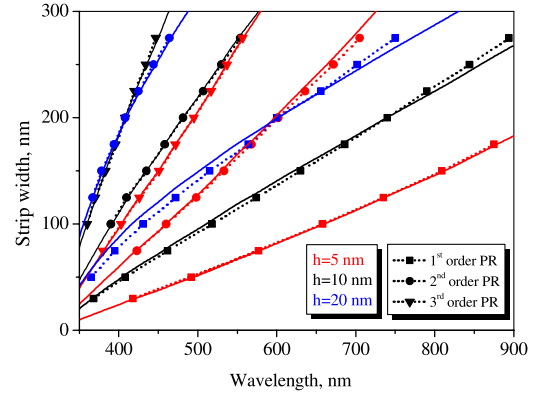


Fig. 6. Resonance strip width as a function of the PR wavelength (first, second, and third orders) for the thickness of 5 (red), 10 (black curves), and 20 nm (blue curves). Points denote the values computed using our method, dashed lines are linear fitting of data, and solid curves are prediction according to (19).

quite accurately the width of the strip providing a PR of prescribed order.

C. Short Grating of Strips

The simplest array is a pair of noble-metal strips. If they are not identical, they should behave as optically coupled nanoscale resonators. In Fig. 2, we demonstrate (by the dotted curves with $d = d_1 + d_2$) the behavior of PRs of two silver strips of identical thickness of 10 nm and the widths of 150 and 168 nm, separated with a 5, 10, and 20 nm gap. As one can see, the coupling invokes a hybridization of the first-order PRs of separately standing silver strips of the same widths.

Multistrip configurations of identical strips are interesting in view of their potential applications in optical antenna arrays and plasmon-assisted solar cells. Their properties are presented in Figs. 7–10.

In Fig. 7, we present the wavelength scans of the normalized TSCS and ACS per one strip for silver and gold multistrip configurations. Here, the total width of a finite strip grating is fixed to be 850 nm and the number of strips is $N = 10$ (i.e., $d = 80.5$ nm and $g = 5$ nm); however, the strip thickness takes three different values. It is seen that making strips thinner shifts the plasmon resonances to the red side. This is because the wavelength of the short-range plasmon wave gets larger for thinner strips [5], [6], see also Fig. 2.

In Fig. 8, the number of strips varies from 1 to 20 by cutting $N-1$ identical gaps of 5 nm each along the 850-nm-wide strip. As one can see, this operation also redshifts the frequency of the most intensive scattering and absorption. Note that the resonances of ACS in Figs. 2, 4, 7, and 8 are a few nanometers shifted from the TSCS maxima and can be close to the latter in magnitude, like in Fig. 2. The largest values of ACS are associated with higher order PRs H_n , $n = 2, 3$ apparently because the bulk losses in silver are considerably larger in the violet part of the visible band than in the red part.

We have also studied the effect of the size of the gap between the strips in a finite flat grating made of identical silver strips on the scattering and absorption of light. The plots of the normalized TSCS and ACS per one strip for the $N = 15$ grating of 300-nm-wide and 5-nm-thin coplanar silver strips, computed

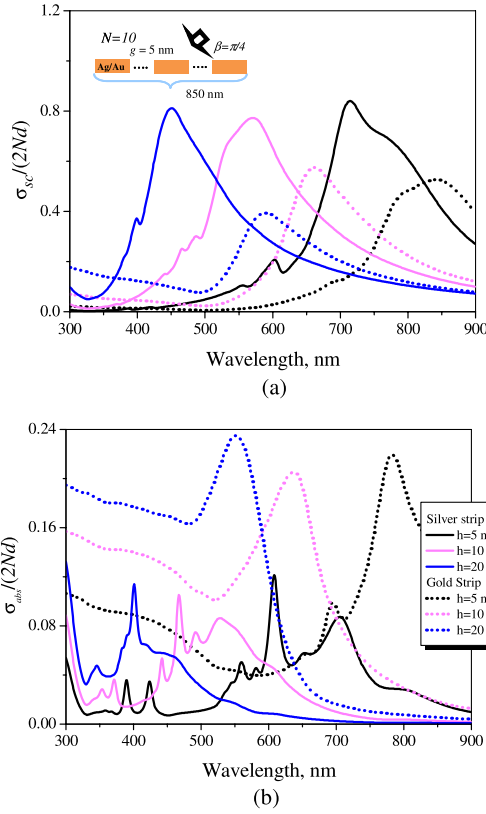


Fig. 7. (a) Normalized TSCS and (b) ACS versus the wavelength for $N = 10$ identical silver and gold strips of varying thickness h separated with 5 nm gaps.

with uniform accuracy of 10^{-4} , are shown in Fig. 9(a) and (b), respectively, as a function of the wavelength at the inclined incidence.

As visible, even if the gaps between the strips are only 5 nm, the optical coupling between the strips is weak. As a result, such configurations support strongly pronounced PRs at the same wavelengths as for a single strip of the same dimensions. In the visible range, the most intensive is the PR H_2 around $\lambda = 735$ nm, while H_1 resonance moves to the infrared range. As already mentioned, ACS can serve as a better than TSCS figure of merit for visualizing higher order PRs.

Fig. 10(a)–(c) displays the total magnetic near-fields and scattering far-field patterns in the second-, third-, and fourth-order PRs, respectively, under the inclined incidence of the H-polarized plane wave on a sparse grating of 15 thin identical coplanar strips.

Here, the taken wavelength values correspond to the maxima on the ACS plot of Fig. 9(b) marked with arrows: $\lambda_{H_2} = 734.05$ nm, $\lambda_{H_3} = 587.05$ nm, and $\lambda_{H_4} = 517.3$ nm. Near each strip, one can see the field hot spots whose number coincides with the index of the corresponding PR. This mechanism is similar to PRs observed on other nanostrip configurations [4]–[8] and also to the PR resonances on 3-D metallic nanorods of finite length [25]. The far-field scattering patterns demonstrate the sharp lobes in the directions close to the angles of propagation of the higher diffraction orders of a relevant infinite grating.

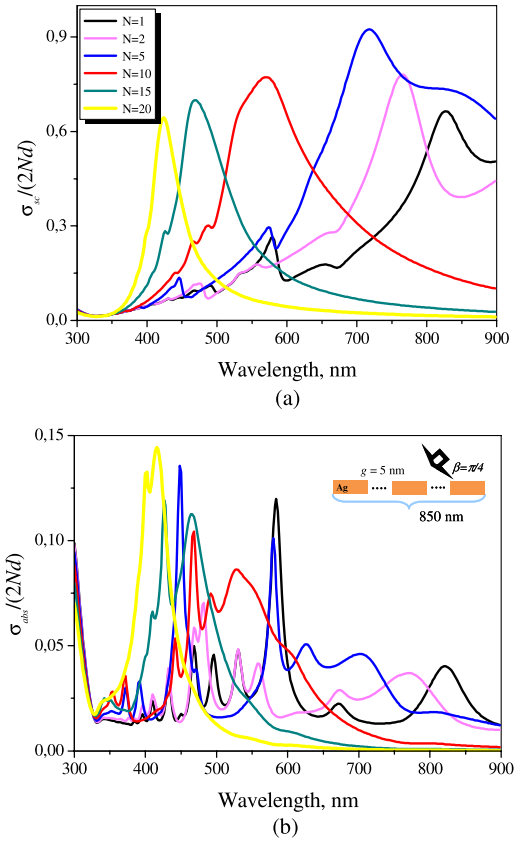


Fig. 8. (a) Normalized TSCS and (b) ACS versus the wavelength for N identical coplanar silver strips of thickness $h = 10$ nm and 5 nm gaps.

D. Long Grating of Strips

If the grating consists of dozens or hundreds of strips, new interesting effect appears, induced by the periodic structuring. In this case, both TSCS and ACS demonstrate a gradual buildup of the grating resonances (GRs) also known as lattice or collective resonances, near to $\lambda_G = p/m$, $m = 1, 2, \dots$ (at normal incidence). This is explained by the existence of specific poles of the field as a function of the wavelength [26], [27].

In Fig. 11, we show the plots of the normalized TSCS versus the wavelength exhibiting two PRs at $\lambda_{H_1} = 633.1$ nm and $\lambda_{H_3} = 379.4$ nm and one GR at $\lambda_G = 450.85$ nm for the grating of $N = 50, 100,$ and 200 strips. As can be seen, if the number of elements in a finite grating gets larger, then the GRs become sharper and approach their limit forms valid for infinite gratings [27].

In Fig. 12, presented are the near-field patterns in the two mentioned PRs around four central strips (from #98 to #101) of the 200-strip grating. They demonstrate bright spots along each strip with maximum magnitudes of 3.3 and 2.6, respectively, rapidly decreasing in the normal direction. At the GR wavelength [see Fig. 13(a)], the near-field pattern is completely different. One can observe an intensive standing wave along the x -axis that has maximum magnitude of 7.8. It is built of the ± 1 -order Floquet harmonics propagating along the plane of grating. In the normal direction, this remarkable standing wave stretches to some ten periods both below and above the grating as seen from the field profiles along the y -axis presented in Fig. 13(b).

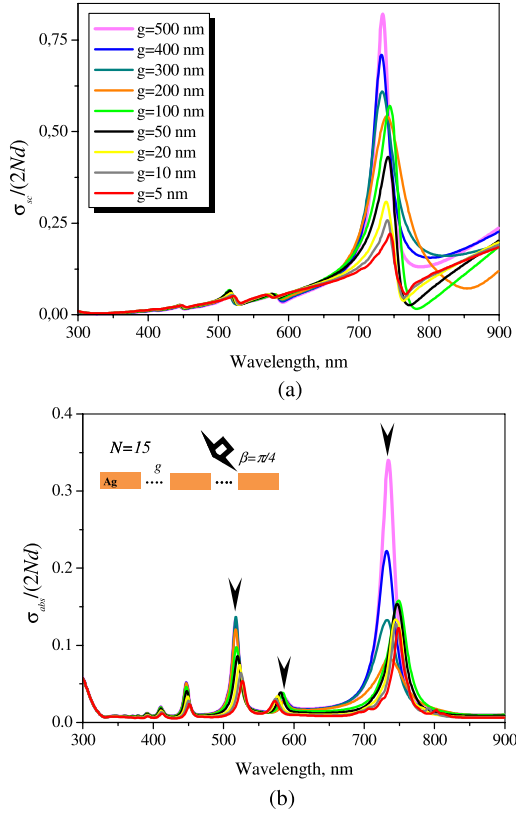


Fig. 9. (a) Normalized TSCS and (b) ACS as a function of the wavelength for $N = 15$ silver strips of width $d = 300$ nm and thickness $h = 5$ nm with different strip gaps for $\beta = \pi/4$, $n_v = n_w = 20$.

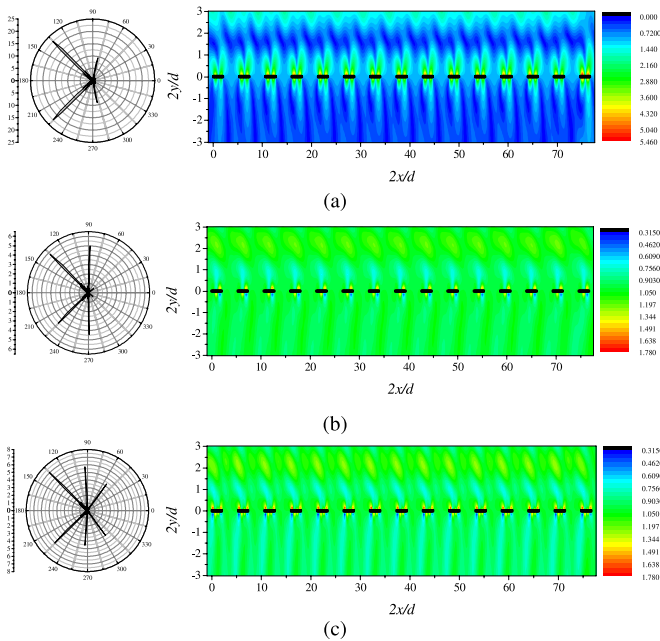


Fig. 10. Total magnetic near-field and scattered far-field patterns at the PR wavelengths (a) $\lambda_{H2} = 734.05$ nm, (b) $\lambda_{H3} = 587.05$ nm, and (c) $\lambda_{H4} = 517.3$ nm for $N = 15$ strips with $d = 30$ nm, $h = 5$ nm, $g = 500$ nm; discretization orders are $n_v = n_w = 20$.

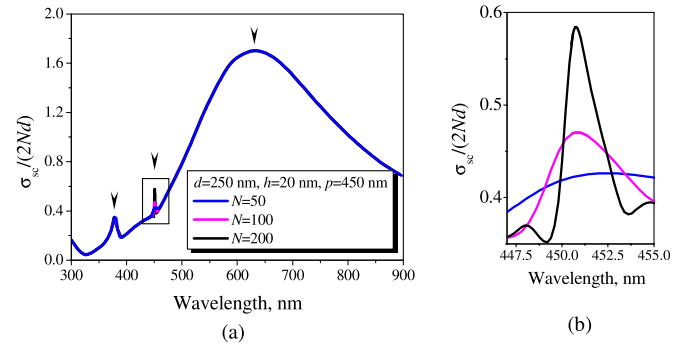


Fig. 11. (a) Normalized TSCS for the normally ($\beta = \pi/2$) incident plane wave by gratings of $N = 50, 100$, and 200 strips of $d = 250$ nm, $h = 20$ nm, and $p = 450$ nm. (b) Zoomed TSCS near the G-resonance wavelengths

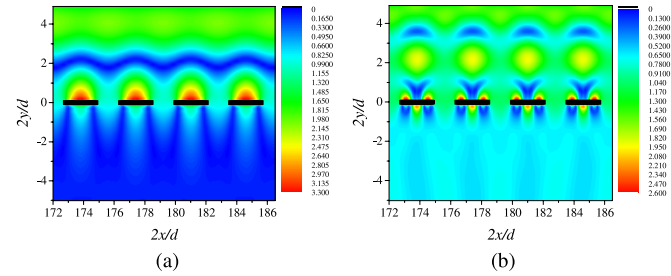


Fig. 12. Magnetic near-field patterns near four central strips in two plasmon resonances. (a) $\lambda_{H1} = 632.3$ nm and (b) $\lambda_{H3} = 379.4$ nm for the same grating as in Fig. 11.

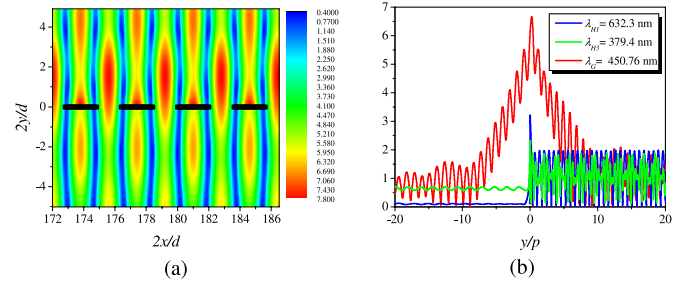


Fig. 13. Magnetic near-field pattern in the G-resonance at (a) $\lambda_G = 450.76$ nm and profiles of the near-field magnitude for the normally incident H-wave, along the grating symmetry line, $x/p = 49.64$ in the G-resonance (red) and along the normal to the central strip, $x/p = 49.28$ in two P-resonances, respectively; other parameters are as in Fig. 11.

This standing wave pattern has been reported in [27] for an infinite grating of silver strips and can be considered as a signature of the GR resonance.

V. CONCLUSION

Summarizing, we have applied a new model and an accurate numerical method to the study of the visible-range plasmon resonances of multiple optically coupled thinner than wavelength silver and gold nanostrip gratings. The model is based on the elimination of the strip internal field with the aid of two-side GBCs imposed on the each strip median line. This leads to two independent sets of coupled IEs, the log-singular and the hypersingular, which we have discretized using the quadratures of interpolation type. The resulting algorithm is efficient

and reliable, with guaranteed convergence and controlled accuracy of computations. Our analysis has shown that this model can potentially replace the contour IE techniques in the whole visible range except, maybe, extreme violet part. Being more economic, it enables modeling of multiple-strip configurations, which offer additional opportunities in the optical engineering of PR-assisted scattering and absorption.

REFERENCES

- [1] J. P. Kottmann and O. J. F. Martin, "Accurate solution of the volume integral equation for high-permittivity scatterers," *IEEE Trans. Antennas Propag.*, vol. 48, no. 11, pp. 1719–1726, 2000.
- [2] G. Schider, J. R. Krenn, W. G. Gotschy, B. Lamprecht, H. Ditlbacher, A. Leitner, and F. R. Aussenegg, "Optical properties of Ag and Au nanowire gratings," *J. Appl. Phys.*, vol. 90, no. 8, pp. 3825–3830, 2001.
- [3] V. Giannini and J. A. Sánchez-Gil, "Calculations of light scattering from isolated and interacting metallic nanowires of arbitrary cross section by means of Green's theorem surface integral equations in parametric form," *J. Opt. Soc. Amer. A*, vol. 24, pp. 2822–2830, 2007.
- [4] T. Søndergaard, "Modeling of plasmonic nanostructures: Green's function integral equation methods," *Phys. Status Solidi (b)*, vol. 244, pp. 3448–3462, 2007.
- [5] T. Søndergaard and S. I. Bozhevolnyi, "Strip and gap plasmon polariton optical resonators," *Phys. Status Solidi (b)*, vol. 245, pp. 9–19, 2008.
- [6] G. Della Valle, T. Søndergaard, and S. I. Bozhevolnyi, "Plasmon-polariton nano-strip resonators: From visible to infra-red," *Opt. Exp.*, vol. 16, no. 10, pp. 6867–6876, 2008.
- [7] M. R. Gadsdon, I. R. Hooper, and J. R. Sambles, "Optical resonances on sub-wavelength lamellar gratings," *Opt. Exp.*, vol. 16, no. 26, pp. 22003–22028, 2008.
- [8] K. C. V. Y. Huang, Y. C. Jun, M.-K. Seo, and M. L. Brongersma, "Power flow from a dipole emitter near an optical antenna," *Opt. Exp.*, vol. 19, no. 20, pp. 19084–19092, 2011.
- [9] A. F. Peterson, "The 'interior resonance' problem associated with surface integral equations of electromagnetics: Numerical consequences and a survey of remedies," *Electromagnetics*, vol. 10, no. 3, pp. 293–312, 1990.
- [10] K. M. Mitzner, "Effective boundary conditions for reflection and transmission by an absorbing shell of arbitrary shape," *IEEE Trans. Antennas Propag.*, vol. 16, no. 6, pp. 706–712, Nov. 1968.
- [11] R. F. Harrington and J. R. Mautz, "An impedance sheet approximation for thin dielectric shells," *IEEE Trans. Antennas Propag.*, vol. 23, no. 4, pp. 531–534, Jul. 1975.
- [12] G. A. Grinberg, "Boundary conditions for the electromagnetic field in the presence of thin metallic shells," *Radio Eng. Electron.*, vol. 26, no. 12, pp. 2493–2499, 1981.
- [13] G. Bouchitté, "Analyse limite de la diffraction d'ondes électromagnétiques par une structure mince," *Proc. C.R. Acad. Paris*, vol. 311, pp. 51–56, 1990.
- [14] E. Bleszynski, M. Bleszynski, and T. Jaroszewicz, "Surface-integral equations for electromagnetic scattering from impenetrable and penetrable sheets," *IEEE Antennas Propag. Mag.*, vol. 35, no. 6, pp. 14–25, Dec. 1993.
- [15] A. Karlsson, "Approximate boundary conditions for thin structures," *IEEE Trans. Antennas Propag.*, vol. 57, no. 1, pp. 144–148, Jan. 2009.
- [16] T. L. Zinenko, A. I. Nosich, and Y. Okuno, "Plane wave scattering and absorption by resistive-strip and dielectric-strip periodic gratings," *IEEE Trans. Antennas Propag.*, vol. 46, no. 10, pp. 1498–1505, Oct. 1998.
- [17] T. L. Zinenko, A. Matsushima, and Y. Okuno, "Scattering and absorption of electromagnetic plane waves by a multilayered resistive strip grating embedded in a dielectric slab," *Trans. IEICE Electron.*, vol. E82-C, no. 12, pp. 2255–2264, 1999.
- [18] T. L. Zinenko and A. I. Nosich, "Plane wave scattering and absorption by flat gratings of impedance strips," *IEEE Trans. Antennas Propag.*, vol. 54, no. 7, pp. 2088–2095, Jul. 2006.
- [19] O. V. Shapoval, R. Sauleau, and A. I. Nosich, "Scattering and absorption of waves by flat material strips analyzed using generalized boundary conditions and Nystrom-type algorithm," *IEEE Trans. Antennas Propag.*, vol. 59, no. 9, pp. 3339–3346, Sep. 2011.
- [20] O. V. Shapoval, R. Sauleau, and A. I. Nosich, "Plasmon resonances in the H-wave scattering by a nanosized thin flat silver strip," in *Proc. Int. Conf. Laser Fiber-Optic Numer. Model.*, Sebastopol, CA, USA, 2010, pp. 37–39.
- [21] O. V. Shapoval, R. Sauleau, and A. I. Nosich, "Coplanar gratings of multiple thin noble-metal nano-strips as surface plasmon resonance structures," presented at the Int. Conf. Transp. Opt. Netw., Stockholm, Sweden, 2011, Paper We.B2.4.
- [22] J. Tsalamengas, "Exponentially converging Nystrom's methods for systems of SIEs with applications to open/closed strip or slot-loaded 2-D structures," *IEEE Trans. Antennas Propag.*, vol. 54, no. 5, pp. 1549–1558, May 2006.
- [23] A. A. Nosich, Y. V. Gandel, T. Magath, and A. Altintas, "Numerical analysis and synthesis of 2D quasi-optical reflectors and beam waveguides based on an integral-equation approach with Nystrom's discretization," *J. Opt. Soc. Amer. A*, vol. 24, pp. 2831–2836, 2007.
- [24] P. B. Johnson and R. W. Christy, "Optical constants of the noble metals," *Phys. Rev. B*, vol. 6, pp. 4370–4379, 1972.
- [25] T. H. Tamianu, F. D. Stefani, and N. F. van Hulst, "Optical nanorod antennas modeled as cavities for dipolar emitters: Evolution of sub- and super-radiant modes," *Nano Lett.*, vol. 11, pp. 1020–1024, 2011.
- [26] D. M. Natarov, V. O. Byelobrov, R. Sauleau, T. M. Benson, and A. I. Nosich, "Periodicity-induced effects in the scattering and absorption of light by infinite and finite gratings of circular silver nanowires," *Opt. Exp.*, vol. 19, no. 22, pp. 22176–22190, 2011.
- [27] T. L. Zinenko, M. Marciniak, and A. I. Nosich, "Accurate analysis of light scattering and absorption by an infinite flat grating of thin silver nanostrips in free space using the method of analytical regularization," *IEEE J. Sel. Topics Quantum Electron.*, vol. 19, no. 3, 2013. DOI: 10.1109/JSTQE.2012.2227685.



Olga V. Shapoval (S'10) was born in Nikopol, Ukraine, in 1987. She received the M.S. (with Hons.) degree in applied mathematics from Kharkiv National University, Kharkiv, Ukraine, in 2009. She is currently working toward the Ph.D. degree in radio physics in the Laboratory of Micro and Nano-Optics, Institute of Radio-Physics and Electronics, National Academy of Science of Ukraine, Kharkiv.

Her current research interests include the scattering problems by strip-like structures, efficient mathematical and numerical solution techniques, and singular and hypersingular integral equations.

Ms. Shapoval was the recipient of the Doctoral Research Award of the IEEE Antennas and Propagation Society in 2010.

Ronan Sauleau (M'04–SM'06) was born in Rennes, France, in 1972. He received the Electronic Engineering and Radiocommunications degree and the French DEA degree in electronics from the Institut National des Sciences Appliquées, Rennes, France, in 1995, the Aggregation degree from Ecole Normale Supérieure de Cachan, Cachan, France, in 1996, and the Doctoral degree in signal processing and telecommunications from the Institut d'Electronique et Telecommunications de Rennes (IETR), University of Rennes 1, Rennes, in 1999.

Since 1999, he has been on the staff of IETR, where since 2009, he has been a Professor. His main research interests include millimeter-wave printed antennas, focusing devices, and periodic structures including electromagnetic bandgap materials and metamaterials.

Dr. Sauleau received the 2004 International Symposium on Antennas and Propagation Conference Young Scientist Travel Grant and the first Young Researcher Prize in Brittany, France, in 2001, for his research on gain-enhanced Fabry–Perot antennas. In 2007, he was elected as a junior member of the Institut Universitaire de France.

Alexander I. Nosich (M'94–SM'95–F'04) was born in Kharkiv, Ukraine, in 1953. He received the M.S., Ph.D., and D.Sc. degrees in radio physics from the Kharkiv National University, Kharkiv, Ukraine, in 1975, 1979, and 1990, respectively.

Since 1979, he has been with the Institute of Radio Physics and Electronics, National Academy of Sciences of Ukraine, Kharkiv, where he is currently a Professor and the Principal Scientist heading the Laboratory of Micro and Nano-Optics. Since 1992, he has held a number of guest fellowship and professorship in the EU, Japan, Singapore, and Turkey. His research interests include the method of analytical regularization, propagation and scattering of waves, open waveguides, antennas, and lasers.

Dr. Nosich was one of the initiators and technical committee Chairman of the International Conference Series on Mathematical Methods in Electro-magnetic Theory. In 1995, he organized the IEEE AP-S East Ukraine Chapter, the first one in the former USSR. He currently represents Ukraine and Georgia in the European Association on Antennas and Propagation.